ELSEVIER

Inner core attenuation anisotropy

Wen-che Yu *, Lianxing Wen

Department of Geosciences, State University of New York at Stony Brook, NY 11794-2100, United States

Abstract

We investigate the attenuation structure of the Earth's inner core and its relationship to the velocity structure globally and along various sampling directions, by studying the amplitude ratios and the differential travel times of the PKiKP–PKIKP and PKPbc–PKIKP phases. Our observations reveal that the amplitude ratios of these core phases, like the differential travel times, vary in both sampling direction and geographic location, and the correlation is ubiquitous between small (large) PKIKP/PKiKP or PKIKP/PKPbc amplitude ratios and large (small) differential PKiKP–PKIKP or PKPbc–PKIKP travel times. These observations indicate that the Earth's inner core is anisotropic in attenuation, and the direction of high (low) attenuation corresponds to that of high (low) velocity. Such anisotropic behaviors can be explained by different alignments of the hexagonal close-packed (hcp) iron crystals under the hypothesis that the hcp iron crystals are anisotropic in attenuation with their axis of high (low) attenuation corresponding to that of high (low) velocity.

© 2006 Elsevier B.V. All rights reserved.

1. Introduction

It is well established that the compressional wave (P wave) velocity in the Earth's inner core varies in both direction and geographic location [1–9]. These inferred seismic velocity structures of the inner core have played an important role in understanding the mineral physics and geodynamics of the inner core [10–18]. The attenuation structure of the inner core is another important constraint in understanding the mineral physics and geodynamics of the inner core. It has been reported that the attenuation structure exhibits complex features [9,19–26] and that a correlation

of high velocity with high attenuation exists in some parts of the inner core [9,22,25,27,28]. However, an overall attenuation structure and its relationship to the velocity structure are not clear. Here, we investigate the attenuation structure of the Earth's inner core and its relationship to the velocity structure, by analyzing the amplitude ratios and differential travel times of the PKiKP–PKIKP and PKPbc–PKIKP phase pairs for the PKIKP waves sampling the inner core globally and along various directions.

2. Seismic data and coverage

Our data sets consist of amplitude ratios and differential travel times of the short-period PKiKP and PKIKP phases observed at the epicentral distance range of 132°–141° and the PKPbc and PKIKP phases recorded at the epicentral distance range of 147.5°–152.5°. PKIKP is

* Corresponding author. Tel.: +1 631 632 1790; fax: +1 631 632 8240.

E-mail addresses: yu@mantle.geo.sunysb.edu (W. Yu), Lianxing.Wen@sunysb.edu (L. Wen).

the P wave transmitted through the inner core; PKiKP is the P wave reflected off the inner core boundary (ICB); and PKPbc is the P wave propagating through the bottom portion of the outer core (Fig. 1a). The amplitude ratios of the PKIKP/PKiKP and PKIKP/PKPbc phases are primarily sensitive to the attenuation structure of the inner
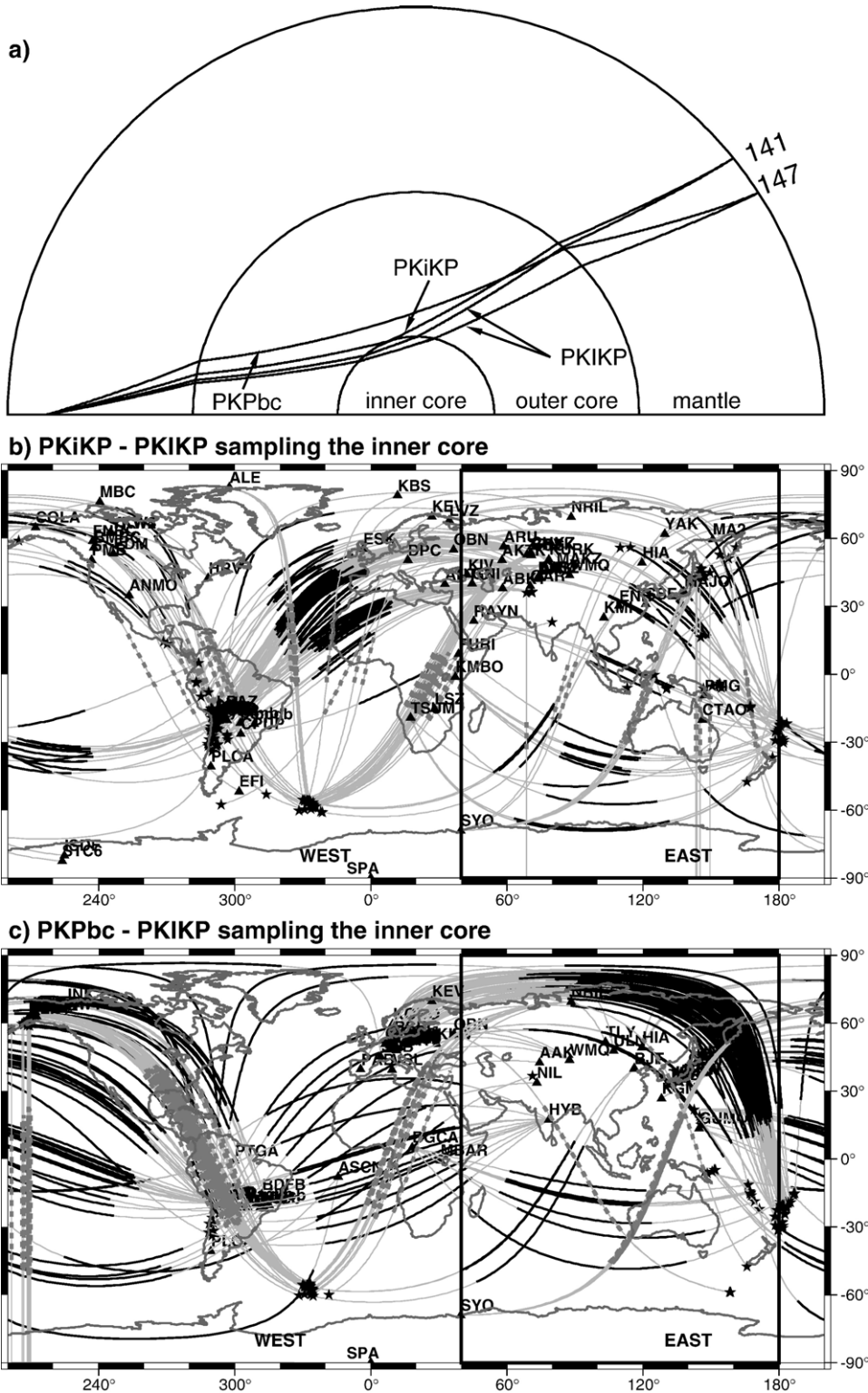
core, as the two phase pairs have similar ray paths in the mantle (Fig. 1a), and there is little attenuation in the outer core. For the same reason, the differential travel times of the PKiKP–PKIKP and PKPbc–PKIKP phases are primarily sensitive to the velocity structure of the inner core. The use of amplitude ratios and differential travel times of the same phase pair also ensures that the attenuation and velocity structures are inferred from the same propagation path in the inner core. In this study, we only use the PKiKP–PKIKP data recorded at the distance range of 132°–141° and the PKPbc–PKIKP data recorded at the distance range of 147.5°–152.5°, which are sensitive to the seismic structures in the top 80 km and 180–290 km of the inner core, respectively. At the distances less than 132°, PKIKP and PKiKP phases interfere with each other, making simple picking of amplitude and travel time implausible (see Fig. 3 of [9]). At the distances less than 147.5°, the differential travel times and amplitude ratios of the PKPbc–PKIKP phases may be affected by the interference of the PKPbc and PKPab phases at the caustic distances (see Fig. 4 of [29]). At the distances larger than 152.5°, the PKPbc waves diffract along the ICB, and the PKIKP/PKPbc amplitude ratios would be affected by the seismic velocity structure at the bottom of the outer core.

Part of the seismic data is the collections from the previous studies [6,8,9,30]. These waveforms are collected from the recordings of the Global Seismographic Network (GSN) of the Incorporated Research Institutions for Seismology (IRIS) Consortium in the time period of 1990–2001, GEOSCOPE, several regional seismic networks in German Regional Seismic Network (GRSN), Grafenberg (GRF), FREESIA, the Brazilian Lithospheric Seismic Project (BLSP), the Broadband Andean Joint Experiment (BANJO), the Seismic Exploration Deep Andes (SEDA), and the Ocean Hemisphere Project (OHP). In this study, the new data sets are assembled from the Kyrgyzstan, the Kazakhstan, the Canadian National Seismograph Network (CNSN), the Broadband Experiment Across Alaskan Range (BEAAR), the Antarctic Microearthquake Project, and the Antarctic Network of Broadband Seismometers. Broadband seismograms are band-pass filtered with the World-Wide Standard Seismograph Network (WWSSN) short-period instrument response, which has a dominant frequency of 1 Hz (see examples of the broadband and short-period

data in Fig. 2). Every seismogram is checked by eyes to ensure its quality. We select our data based on the simplicity of earthquake source and good signal-to-noise ratio. A total of 222 PKiKP–PKIKP and 254 PKPbc–PKIKP high quality phase pairs are selected from a collection of more than 16,000 seismograms. The selected seismic data have good global coverage and sample along both polar (the paths that have an angle less than 35° between the PKIKP ray direction in the inner core turning point and the Earth's rotation axis) and equatorial (the paths that have an angle greater than 35° between the PKIKP ray direction in the inner core turning point and the Earth's rotation axis) paths. Top portion of the inner core is well sampled along equatorial paths, but relatively poorly sampled along polar paths (Fig. 1b, c). The sampling along polar paths is mainly restricted by the fact that both earthquakes and seismographs must be at high latitudes. Our polar data are collected from events occurring in the South Sandwich Islands, the Macquarie Ridge, and the New Zealand in the Southern Hemisphere, and the Kurile Island, the Kamchatka, Alaska, and the Russia in the Northern Hemisphere. The amplitude ratios and differential travel times are measured based on the relative magnitudes and time separations between the maximum amplitudes of the phase pairs. The travel time measurement is proved to be comparable to that determined from the waveform cross-correlation and the difference in travel time measurement between the two methods is less than 0.05 s. The differential travel time residuals are obtained from the observed differential travel times relative to the predicted ones on the basis of the Preliminary Reference Earth Model (PREM) [31]. The observed amplitude ratios are corrected for the radiation patterns of the earthquake sources, although the effect is very small due to the similar take-off angles of the phase pairs.

3. Seismic observations and models

Our observed differential travel time residuals exhibit variations in both sampling direction and geographic location, consistent with previous results [1–9]. The differential travel time residuals are, in general, larger for the PKIKP waves sampling along polar paths than for those along equatorial paths, and the magnitudes of this polar–equatorial difference are different between the "eastern" and "western" hemispheres (Fig. 3a, c and

Fig. 1. (a) PKP ray paths based on the Preliminary Reference Earth Model (PREM) [31]: PKiKP, PKIKP at an epicentral distance of 141° and PKPbc, PKIKP at 147°. (b, c) Map view of great-circle paths (light gray lines) and ray segments of the PKIKP phases sampling the inner core for the observed PKiKP–PKIKP phases (b) and the PKPbc–PKIKP phases (c). Equatorial and polar ray segments in the inner core are indicated by black solid and dark gray broken lines, respectively. Stars and triangles indicate locations of earthquakes and seismic stations, respectively. The geographic region of the two hemispheres is marked, with the eastern hemisphere defined between 40°E and 180°E and the western hemisphere defined between 180°W and 40°E.

examples of waveforms in Fig. 2). The "eastern hemisphere" is defined for which the PKIKP ray segment in the inner core is within 40°E–180°E; and the "western hemisphere" is defined for which the PKIKP ray segment in the inner core is within 180°W–40°E. In the following text, the "eastern" and "western" hemispheres are referred to the regions we define. Note that, the differential travel time residuals of the PKPbc–PKIKP phases along polar
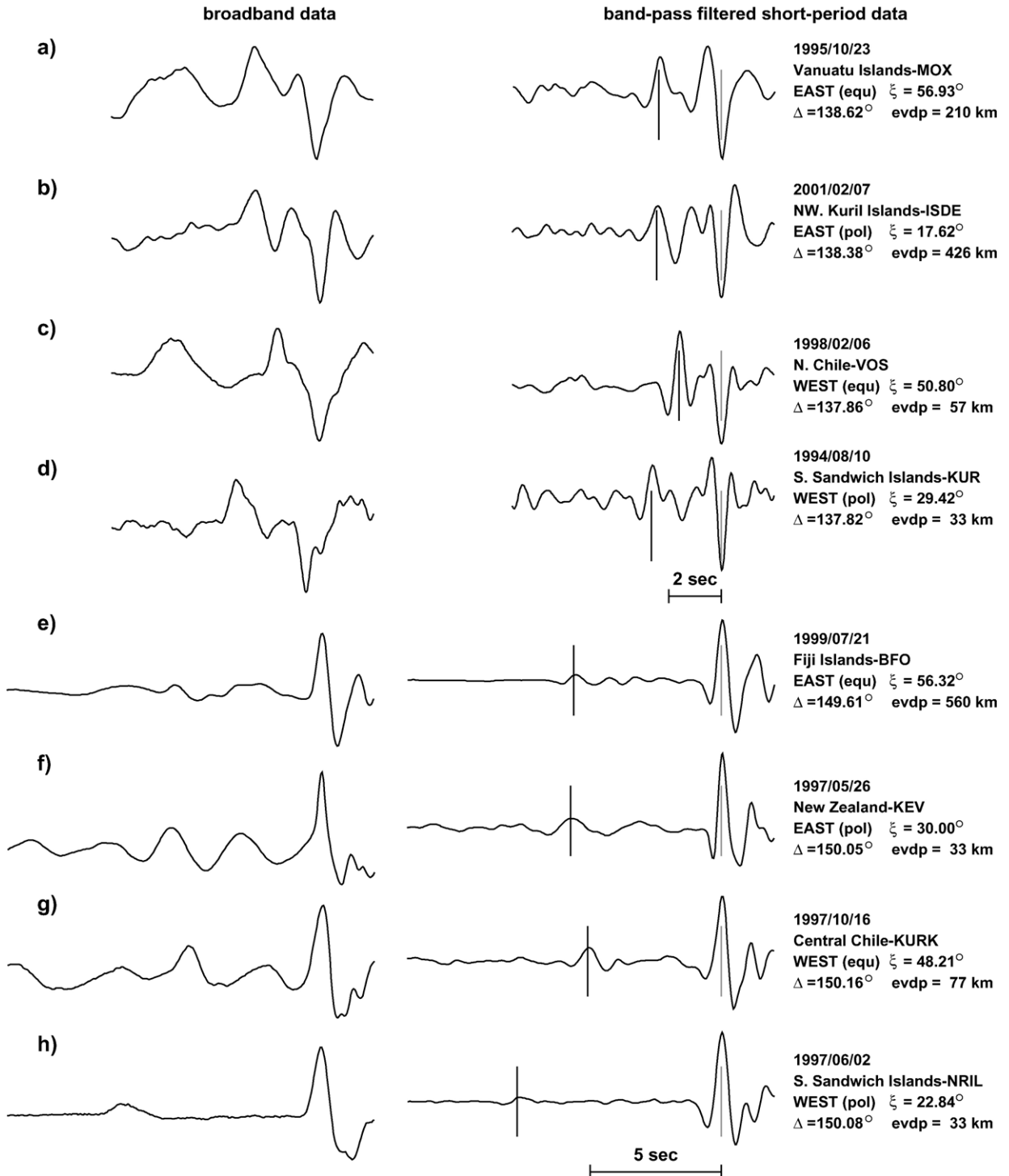
paths (blue solid triangles, Fig. 3c) are about 3–4 s larger than those along equatorial paths (black open triangles, Fig. 3c) for the PKIKP waves sampling the western hemisphere (see also examples of waveforms in Fig. 2g, h). The observed PKiKP–PKIKP differential travel time residuals exhibit regional variations in polar–equatorial difference for the PKIKP waves sampling the western hemisphere. In a localized region beneath Africa, the differential travel time residuals along polar paths (blue solid triangles, Fig. 3a) are about 0.7–1.2 s larger than those along equatorial paths (black open triangles, Fig. 3a; see also examples of waveforms in Fig. 2c, d), while, in most regions of the western hemisphere (the middle Atlantic Ocean, Central America, the Caribbean Sea), the differential travel time residuals do not show noticeable polar–equatorial differences (green solid and black open triangles for the polar and equatorial data, respectively, Fig. 3a). The polar–equatorial difference in differential travel time residuals for the PKIKP waves sampling the eastern hemisphere is non-existent at distances less than 150° (red and black solid circles for the polar and equatorial data in Fig. 3a, c; see also examples of PKiKP–PKIKP waveforms in Fig. 2a, b and PKPbc–PKIKP waveforms in Fig. 2e, f). Along equatorial paths, the PKiKP–PKIKP and PKPbc–PKIKP differential travel time residuals also exhibit east–west hemispheric differences. The differential travel time residuals for the PKIKP waves sampling the eastern hemisphere (black solid circles, Fig. 3a, c) are about 0.7 s larger than for those sampling the western hemisphere (black open triangles, Fig. 3a, c; see also examples of PKiKP–PKIKP waveforms in Fig. 2a, c and PKPbc–PKIKP waveforms in Fig. 2e, g).

The observed differential travel time residuals reflect velocity variations in the inner core. Large (small) differential travel time residuals would indicate high (low) velocities in the inner core. The velocity models E1 and W2, appropriate for explaining the seismic data sampling the eastern and western hemispheres along equatorial paths, respectively, have been resolved from the joint modeling of the PKiKP–PKIKP waveforms and the PKPbc–PKIKP differential travel time residuals [9,29,30] (see gray line labeled as E1 and black solid

line labeled as W2 in Fig. 3a, c for predictions). Readers are referred to these papers for the detailed discussions. E1 (for the eastern hemisphere) has PREM velocity in the bottom of the outer core and a coupled small velocity gradient in the top 235 km, followed by a steep transition in the depth range of 235–375 km below the ICB; W2 (for the western hemisphere) has a low velocity gradient OW in the bottom of the outer core and a coupled steep velocity gradient in the top of the inner core (see Fig. 6 of [29] and Fig. 6a of [30] for the velocity structures of E1 and W2). OW has reduced velocities relative to PREM linearly decreasing from 0% at 200 km above the ICB to -0.35% at the ICB [29]. E1 velocity is about 1% higher than W2 in the top 200 km of the inner core. Along polar paths in the eastern hemisphere, because the observed differential travel time residuals exhibit no difference from those sampling equatorial paths until at a distance of about 150°, the differential travel time residuals can be, to the first order, explained by E1 (see gray line labeled as E1 in Fig. 3a, c for predictions). In other words, there is no velocity anisotropy in the top 200 km of the inner core in the eastern hemisphere, consistent with the results in the previous studies [8]. Along polar paths in most regions of the western hemisphere where the PKiKP–PKIKP differential travel time residuals do not exhibit polar–equatorial differences, the differential travel time residuals can be explained by W2 (see black solid line labeled as W2 in Fig. 3a for predictions). This indicates no velocity anisotropy in the top 80 km of the inner core in most regions of the western hemisphere, consistent with previous results [2,4,7]. In a localized region beneath Africa and in the deeper part of the inner core beneath the western hemisphere, the polar differential travel time residuals can be explained by an anisotropy velocity model W2A (see black dotted line labeled as W2A in Fig. 3a, c for predictions). W2A has an increasing magnitude of velocity anisotropy relative to W2 from 1.3% at the ICB to 2.8% at 280 km below the ICB. Such increase of anisotropy with depth is required by the seismic data. Note that models with uniform anisotropy cannot explain both the PKiKP–PKIKP and PKPbc–PKIKP differential travel time residuals. While

Fig. 2. Examples of the broadband (left panel) and band-pass filtered short-period vertical displacements (right panel). The PKIKP and PKiKP phases are shown in (a–d) and the PKIKP and PKPbc phases are shown in (e–h). For comparison, the data recorded at approximately same distances, but with different sampling directions and geographic locations, are selected. Event date, event location–seismic station, PKIKP sampling region and direction (for example, EAST (equ) is the PKIKP ray sampling the eastern hemisphere of the inner core along equatorial path), PKIKP ray angle relative to the Earth's rotation axis (ξ), epicentral distance (Δ), and event depth (evdp) are labeled in the right panel. Short-period data are obtained from deconvolving the broadband raw data with the instrument response, band-pass filtering in the frequency range of 0.005 Hz–4 Hz, and convolving with the WWSSN short-period instrument response with a dominant frequency of 1 Hz. The maximum amplitudes of the PKIKP and PKiKP (PKPbc) phases are marked by the black and gray bars, respectively. Note that the polarity of PKiKP is opposite to that of PKIKP, due to the wide-angle reflection of the PKiKP phase.

a uniform anisotropy of 1.3% can generally explain the PKiKP–PKIKP data, it underestimates the PKPbc–PKIKP differential travel time residuals (see black

dotted line labeled as 1.3% in Fig. 3a, c for predictions). On the other hand, while a uniform anisotropy of 2.8% predicts generally well the PKPbc–PKIKP data, it over-
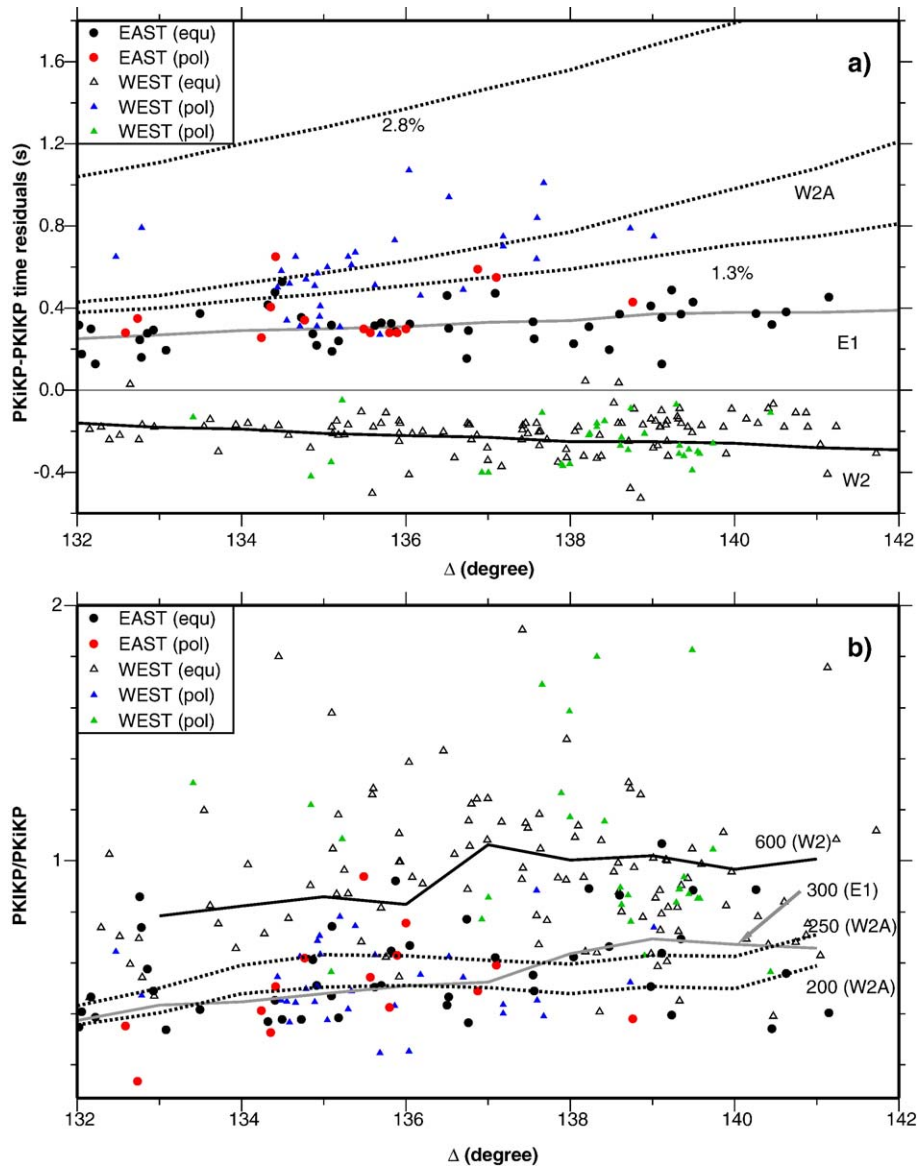

Fig. 3. (a) Observed PKiKP–PKIKP and (c) PKPbc–PKIKP differential travel time residuals relative to PREM as a function of epicentral distance (Δ), along with the predicted differential travel time residuals based on E1 (gray line), W2 (black solid line), W2A (black dotted line), and models with velocities being 1.3% and 2.8% higher than W2 (black dotted lines labeled as 1.3% and 2.8%). E1 is about 1% higher than W2 [9,29,30]. W2A has a linearly increasing velocity structure relative to W2 from 1.3% at the ICB to 2.8% at 280 km below the ICB. (b) Observed PKIKP/PKiKP and (d) PKIKP/PKPbc amplitude ratios as a function of epicentral distance (Δ), along with the predicted amplitude ratios based on several attenuation models of the inner core and their associated coupled outer core–inner core velocity models labeled as Q value (velocity model) (for example, 300 (E1) is predicted based on a model with a Q value of 300 and the velocity model E1). The meaning of the symbol is shown in the inset. Blue (green) solid triangles represent the PKiKP–PKIKP data along polar paths sampling a localized region beneath Africa (the middle Atlantic Ocean, Central America, the Caribbean Sea) of the western hemisphere (a, b). Predicted amplitude ratios are obtained from handpicking the maximum amplitudes of the PKIKP and PKiKP phases (b) or PKPbc phases (d) of the synthetic waveforms, calculated using the generalized ray theory [32]. Distance corrections are made so that the differential travel time residuals and amplitude ratios are plotted at the distances equivalent to a source depth of 200 km. Accordingly, the predicted differential travel time residuals and amplitude ratios are computed based on a source depth of 200 km.
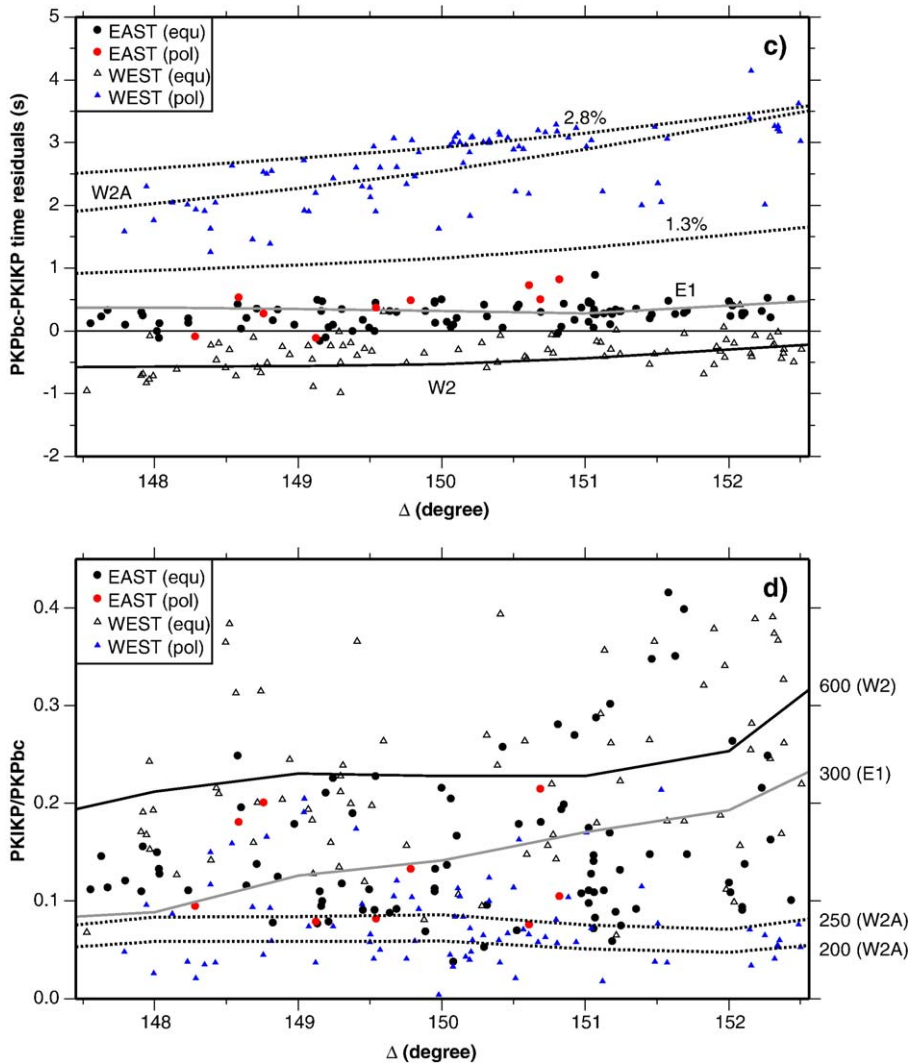
Fig. 3 (*continued*).

predicts the PKiKP–PKIKP differential travel time residuals (see black dotted line labeled as 2.8% in Fig. 3a, c for predictions).

The observed amplitude ratios exhibit variations strongly resembling those of differential travel time residuals in both the sampling direction and geographic location. Small (large) amplitude ratios are observed for the data exhibiting large (small) differential travel time residuals (Fig. 3 and examples of waveforms in Fig. 2). Along polar paths in the western hemisphere, where the observed differential travel time residuals of the PKiKP–PKIKP and PKPbc–PKIKP phases are much larger than those along equatorial paths (blue solid and black open triangles, Fig. 3a, c), the observed amplitude ratios are much smaller than those along equatorial paths (same symbols, Fig. 3b, d; see also examples of the equatorial

and polar PKiKP–PKIKP waveforms in Fig. 2c, d and the equatorial and polar PKPbc–PKIKP waveforms in Fig. 2g, h). For the region in the western hemisphere where the polar–equatorial difference in PKiKP–PKIKP differential travel time residual is non-existent (green solid and black open triangles, Fig. 3a), the PKIKP/PKiKP amplitude ratios do not show noticeable polar–equatorial difference either (same symbols, Fig. 3b). Along polar paths in the eastern hemisphere, where the differential travel time residuals are similar to those along equatorial paths (red and black solid circles, Fig. 3a, c), the amplitude ratios are indistinguishable between equatorial and polar paths (same symbols, Fig. 3b, d; see also examples of the equatorial and polar PKiKP–PKIKP waveforms in Fig. 2a, b and the equatorial and polar PKPbc–PKIKP waveforms in Fig. 2e, f). Along

equatorial paths in the eastern hemisphere, where the differential travel time residuals (black solid circles, Fig. 3a, c) are about 0.7 s larger than those in the western hemisphere (black open triangles, Fig. 3a, c), the amplitude ratios are on average smaller than those observed in the western hemisphere (same symbols, Fig. 3b, d; see also examples of the equatorial PKiKP–PKIKP waveforms sampling the eastern and western hemispheres in Fig. 2a, c and the equatorial PKPbc–PKIKP waveforms sampling the eastern and western hemispheres in Fig. 2e, g).

The PKIKP/PKiKP and PKIKP/PKPbc amplitude ratios are primarily sensitive to the attenuation structure of the inner core. Smaller amplitude ratios would indicate smaller amplitudes of the PKIKP phases, and thus higher attenuation in the part of the inner core they sample. The above observations indicate that the inner core is anisotropic in attenuation, with the direction of high attenuation corresponding to that of high velocity. Attenuation is usually represented by quality factor Q, which is defined as fractional loss of energy per cycle of wave oscillation as seismic waves travel through the medium. Attenuation structures in the inner core can be derived from fitting the observed amplitude ratios of the PKIKP/PKiKP and PKIKP/PKPbc phases. Because the PKiKP and PKIKP amplitudes are sensitive to the velocity structure in the bottom of the outer core and the top of the inner core, our Q values are inferred based on the associated velocity models that well explain the PKiKP–PKIKP waveforms and the PKPbc–PKIKP differential travel time residuals for the PKIKP waves sampling different directions and different regions of the inner core. Predicted amplitude ratios are obtained from the handpicked the maximum amplitudes of the PKIKP and PKiKP (PKPbc) phases of the synthetic waveforms, calculated using the generalized ray theory method [32]. In this study, we adopt simple uniform Q values to fit both data sets. Because the seismic observations have been filtered with the WWSSN short-period instrument response, our inferred attenuation structures are appropriate at about 1 Hz, the dominant frequency of the

instrument response. The attenuation structures for the eastern and western hemispheres along equatorial paths are derived and discussed elsewhere [9,30]. The attenuation structure for the eastern hemisphere has an average Q value of 300 in the top 300 km and an average Q value of 600 in the deeper part of the inner core; the attenuation structure for the western hemisphere has an average Q value of 600 in the top 400 km of the inner core (Fig. 6b of [30]). Because the observed amplitude ratios of the PKIKP/PKiKP phases and the PKIKP/PKPbc phases at the distance range of 147.5°–152.5° do not require a depth-dependent attenuation structure for the eastern hemisphere, we adopt a uniform Q value of 300 for the eastern hemisphere. A Q value of 300 (see gray line labeled as 300 (E1) in Fig. 3b, d for predictions) can explain the amplitude ratios along both equatorial and polar paths for the PKIKP waves sampling the eastern hemisphere (black and red solid circles, Fig. 3b, d). A Q value of 600 (see black solid line labeled as 600 (W2) in Fig. 3b, d for predictions) can account for the amplitude ratios along equatorial paths for the PKIKP waves sampling the western hemisphere (black open triangles, Fig. 3b, d) and the PKIKP/PKiKP amplitude ratios along polar paths for the PKIKP waves sampling most regions of the western hemisphere (the middle Atlantic Ocean, Central America, the Caribbean Sea) (green solid triangles, Fig. 3b). A Q value of about 200–250 (see black dotted lines labeled as 200 (W2A) and 250 (W2A) in Fig. 3b, d for predictions) can explain the PKIKP/PKiKP amplitude ratios along polar paths for the PKIKP waves sampling the region beneath Africa (blue solid triangles, Fig. 3b) and the PKIKP/PKPbc amplitude ratios along polar paths for the PKIKP waves sampling the western hemisphere (blue solid triangles, Fig. 3d).

Averages and standard deviations of the observations can be used to estimate the uncertainties of the velocity and attenuation models. Along equatorial paths, most averages and standard deviations of the observed differential time residuals are within the predictions of $\pm 0.1\%$ velocity perturbations from the best-fitting velocity models E1, W2 (Fig. 4a, c, e, g), indicating the

Fig. 4. (a, b, c, d) Average observed differential travel time residuals of the PKiKP–PKIKP (a) and PKPbc–PKIKP (c) phases and amplitude ratios of the PKIKP/PKiKP (b) and PKIKP/PKPbc (d) phases sampling the eastern hemisphere, along with the standard deviations and predictions based on the best-fitting velocity and attenuation model and models perturbed from the best-fitting model. Panels (e, f, g, h) similar to (a, b, c, d) but for the PKiKP–PKIKP and PKPbc–PKIKP phases sampling the western hemisphere. Solid and open symbols represent the averages of the data sampling along equatorial and polar paths, respectively. Black solid lines and gray dotted lines represent the predictions of the best-fitting velocity and attenuation model and models perturbed from the best-fitting model, respectively. Prediction of the perturbed velocity model is labeled as the best-fitting velocity model with the percent perturbation of velocity. For instance, E1 − 0.1% stands for the predictions based on a model with velocities −0.1% lower than E1. Prediction of the perturbed attenuation model is labeled as Q value (the associated best-fitting velocity model). For instance, 250 (E1) represents the predicted amplitude ratios based on a Q value of 250 and an associated velocity model E1. (f) Prediction of 5000–100 (W2) is based on Q values decreasing from 5000 at the ICB to 100 at 80 km below the ICB and an associated velocity model W2. Only the standard deviations of the averages with data points being greater than 1 are plotted.
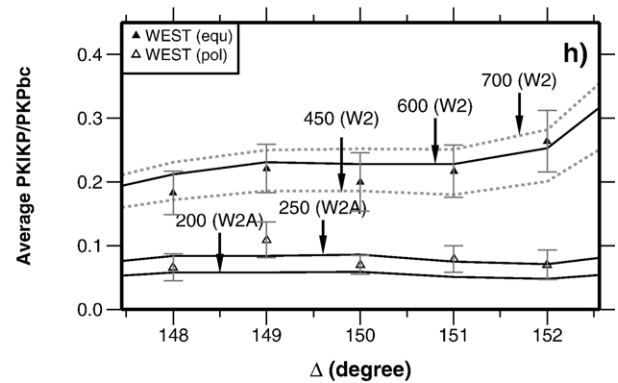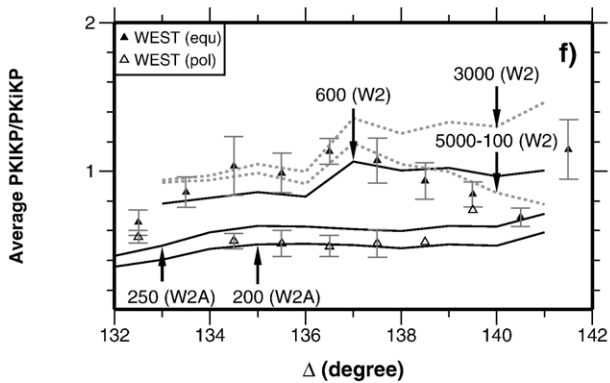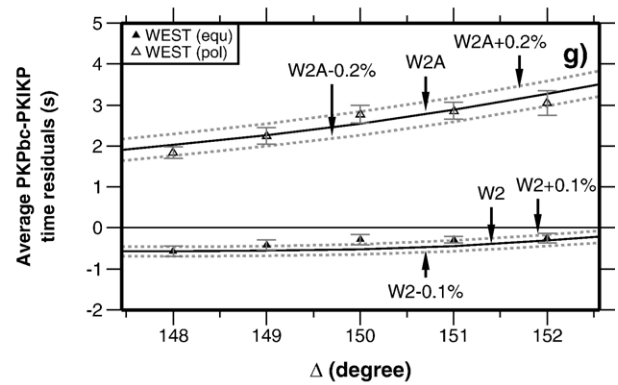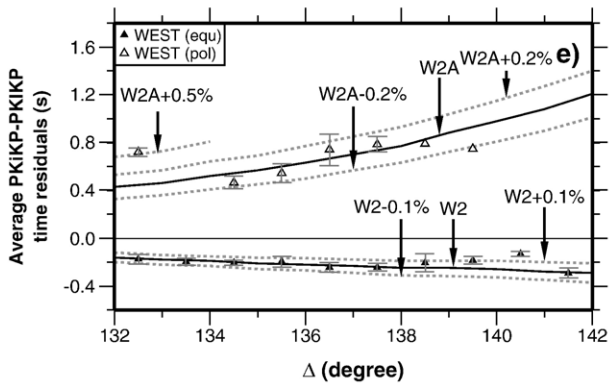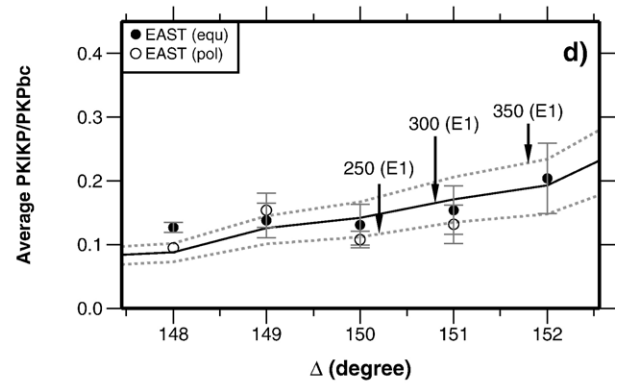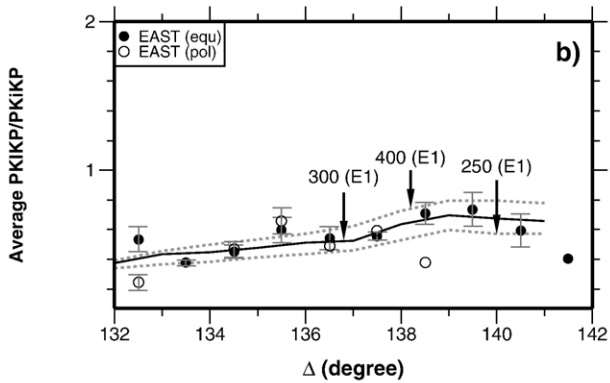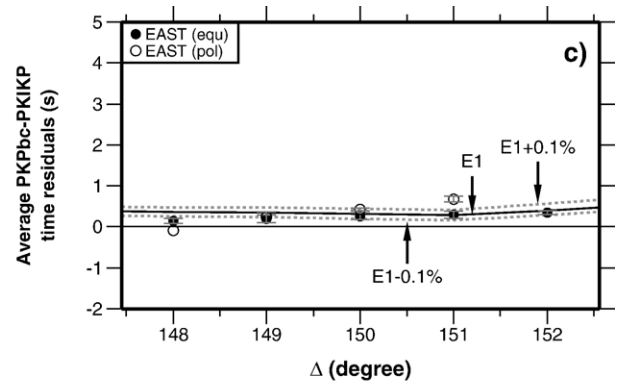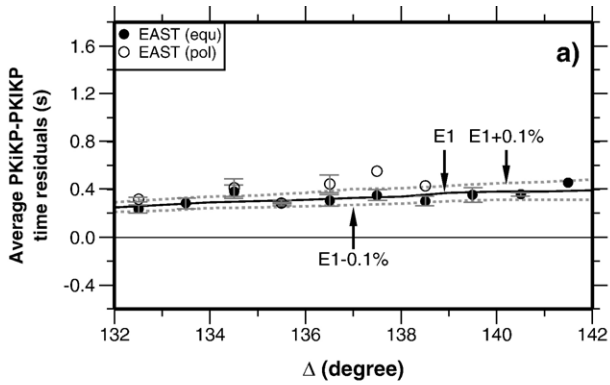
level of heterogeneity in isotropic velocity structure is low within each of the hemispheres. Along polar paths in the western hemisphere, averages and standard deviations of the observed differential time residuals constrain the uncertainties of the velocity model to be within −0.2% to +0.5% of W2A (Fig. 4e, g), suggesting complex anisotropic velocity structures. In the eastern hemisphere, averages and standard deviations of the observed amplitude ratios are within the predictions of Q values between 250 and 400 (Fig. 4b, d). Along equatorial paths in the western hemisphere, averages and standard deviations of the observed PKIKP/PKPbc amplitude ratios are within the predictions of Q values between 450 and 700, while averages and standard deviations of the observed PKIKP/PKiKP amplitude ratios are far deviated from the predictions of Q values within a range of 600–3000 (Fig. 4f). An attenuation structure similar to the model proposed by Cao and Romanowicz [26], having Q values decreasing from 5000 at the ICB to 100 at 80 km below the ICB, could explain the trend of the average PKIKP/PKiKP observations (Fig. 4f). However, such an attenuation structure would under-predict the PKIKP/PKPbc amplitude ratios at larger distances. Along polar paths in the western hemisphere, most averages and standard deviations of the observed amplitude ratios constrain the Q value to be about 200–250 (Fig. 4f, h).

In other words, in the regions of the western hemisphere that exhibit anisotropy, the attenuation anisotropy can be represented by a Q value of about 200–250 along polar paths and an average Q value of 600 along equatorial paths. This attenuation anisotropy corresponds to a polar–equatorial velocity anisotropy with the polar paths being 1.3%–2.8% higher than the equatorial paths. Along equatorial paths, the attenuation structure has an east–west hemispheric variation with an average Q value of 300 in the eastern hemisphere and an average Q value of 600 in the western hemisphere. Such a hemispheric variation in attenuation corresponds to a hemispheric difference in velocity with the velocity in the eastern hemisphere being about 1% higher than that in the western hemisphere.

4. Discussions

4.1. Mantle effect

The above observations can unlikely be explained by the seismic heterogeneities near the core–mantle boundary (CMB). The Fresnel zone of these core phases is about 150 km at the CMB for the P waves we use with a dominant frequency of 1 Hz. For the PKiKP–PKIKP phases, the separations between two ray paths are about 50 km at the CMB, and the Fresnel zones of these two phases overlap (Fig. 5a). For the PKPbc–PKIKP phases, the separations between two ray paths at the CMB are about 300 km, about double the size of the Fresnel zone (Fig. 5b). It is difficult to correct for the mantle effects as small-scale heterogeneities are not well known. It would, however, be contrived that small-scale seismic heterogeneities at the CMB would preferentially affect one branch of these core phase pairs in one particular region or in one particular sampling direction in a hemispheric scale. In fact, dense observations would allow us to exclude the possibility that the signals observed in the PKPbc–PKIKP data are originated from the CMB. Note that, in the regions sampled by dense observations, the Fresnel zones of the PKIKP and PKPbc phases overlap at the CMB (Fig. 5b). Seismic heterogeneities at the CMB would affect the travel times and amplitudes of the PKIKP and PKPbc phases in the same way, and thus cannot provide an explanation for the observed differential travel times and amplitude ratios. The consistency between the observed PKiKP–PKIKP and PKPbc–PKIKP data provides another line of evidence that amplitude ratios and differential travel times of these core phase pairs mainly reflect the signals originated from the seismic structures in the inner core.

4.2. Effect of velocity anisotropy on PKIKP amplitudes

The PKIKP amplitudes would also be affected by the wave propagation in a medium with velocity anisotropy. The velocity anisotropy would distort the wave front, and thus produce focusing or defocusing of wave energy along the wave propagation. Such effects, however, may be small for a small magnitude of velocity anisotropy [33]. To the first order, we have ignored such effects in deriving our attenuation models of the inner core. Further studies on the effect of velocity anisotropy for these core phases are warranted, however.

4.3. Comparisons with previous studies

Inner core attenuation anisotropy and the velocity–attenuation relationship were studied by several previous studies [23,25,27,28]. These studies were based on the analyses of the differential travel times and amplitude ratios of the PKPbc–PKIKP phases [25,27,28] or inversion for the PKIKP waveforms [23]. Overall, our observed equatorial–polar difference of the PKPbc–PKIKP differential travel times and the PKIKP/PKPbc amplitude ratios is consistent with the results in the previous studies (see, for example, Fig. 3 of [27] and Fig. 8 of [28]). Compared to the previous studies, our study has included the PKiKP–
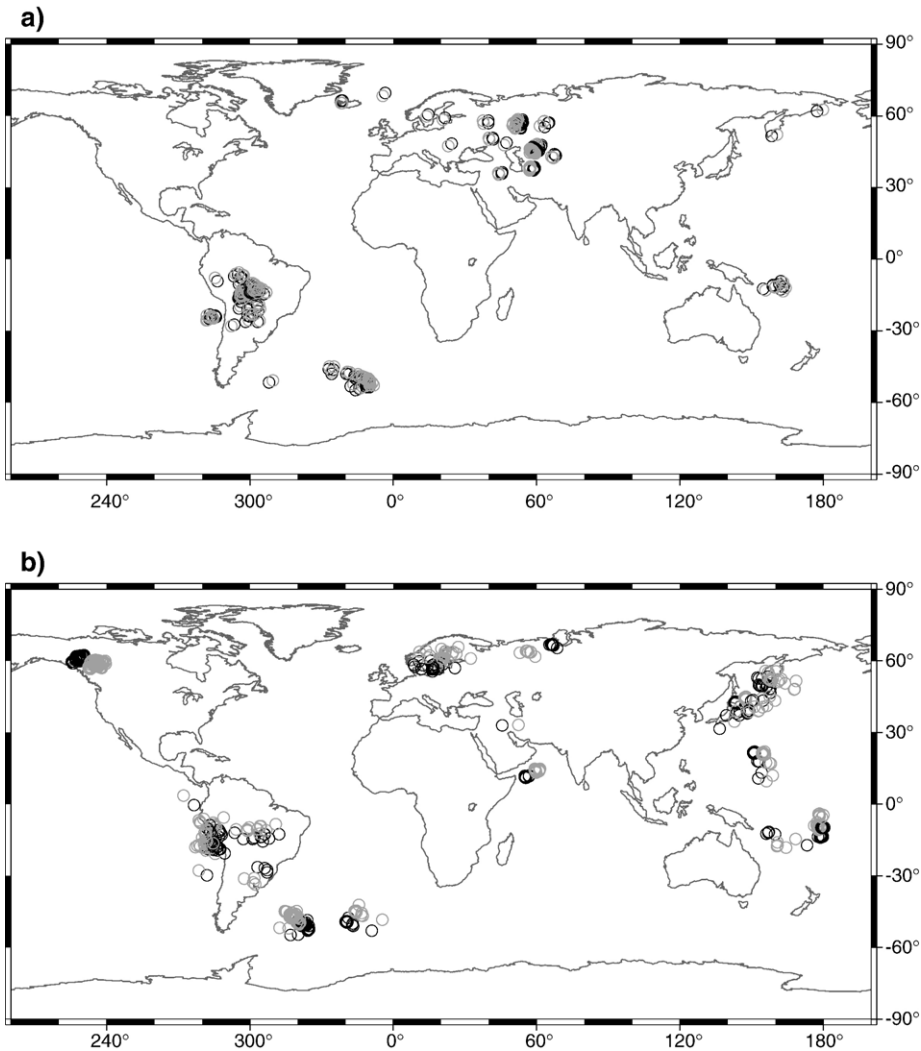
Fig. 5. The entry and exit points at the core–mantle boundary (CMB) for the PKiKP and PKIKP phases (a) and the PKPbc and PKIKP phases (b) for some regions with dense observations. Black and light gray circles represent the hit points at the CMB for the PKIKP and PKiKP (PKPbc) phases (a). These data sets are collected from the regional seismic networks: BLSP, BANJO, SEDA (a, b), Kazakhstan (a), Kyrgyzstan (a), FREESIA (b), GRF and GRSN (b), BEAAR (b), and the GSN stations COL, NRIL (b). The size of the circles is equivalent to the size of the Fresnel zones of the short-period PKP waves at the CMB. The Fresnel zones of the PKiKP and PKIKP phases overlap at the CMB (a). The Fresnel zones of the PKIKP and PKPbc phases overlap in the regions sampled by dense observations (b).

PKIKP data; it also reveals a hemispheric difference in both attenuation and velocity, and the correlation of high (low) velocity and high (low) attenuation between the two hemispheres along equatorial paths. The PKiKP–PKIKP data allow the seismic velocity and attenuation structures in top 80 km of the inner core to be studied. The joint analyses of both the PKiKP–PKIKP and PKPbc–PKIKP phases also allow us to resolve the depth dependence of attenuation and velocity relationship in the inner core. Indeed, the PKPbc–PKIKP data alone do not have resolution to resolve the depth dependence of the seismic structures in the top 300 km of the inner core, making the interpretations of the

observed correlation of differential travel times and amplitude ratios ambiguous. Take the PKIKP/PKPbc observations sampling the western hemisphere as an example. Based on those PKIKP/PKPbc observations alone, the observed small PKIKP/PKPbc amplitude ratios along polar paths could be caused by strong attenuation in the top 80 km of the inner core, while their large differential travel times could be caused by strong velocity anisotropy in the deeper part of the inner core. Incorporating the PKiKP–PKIKP data not only presents a complete picture of the seismic velocity and attenuation structures in the top 300 km of the inner core, but also resolves unambiguously

that the observed differential travel times and amplitude ratios are caused by the same portion of the inner core. Our observations that the correlation of high (low) velocity with high (low) attenuation exists not only for the polar–equatorial paths but also for the two hemispheres along equatorial paths suggest that such velocity–attenuation correlation is ubiquitous in the inner core.

4.4. Inner core velocity and attenuation anisotropy in three dimensions

While the correlation between high (low) velocity and high (low) attenuation appears to be ubiquitous in the inner core, the actual anisotropic pattern is complex in three dimensions. We have made significant effort searching for the PKIKP rays sampling along polar paths. The PKiKP–PKIKP and PKPbc–PKIKP data along polar paths sample Australia, the Indian Ocean, the western Pacific beneath the eastern hemisphere, and Africa, the middle Atlantic Ocean, the Caribbean Sea, Central America, and the Central Pacific beneath the western hemisphere (Fig. 1b, c). The velocity and attenuation anisotropy beneath the eastern hemisphere appears to be non-existent in the top 200 km of the inner core (see also [8]). The velocity and attenuation anisotropy beneath the western hemisphere is complex and exhibits regional variations. The velocity and attenuation anisotropy beneath Africa appears to be strong and present in the top 80 km of the inner core, while no velocity and attenuation anisotropy is observed beneath the Caribbean Sea and Central America in the same depth range of the inner core. The velocity and attenuation anisotropy beneath the Caribbean Sea and Central America becomes strong about 180 km below the inner core (see also [2,4,7]). There is no constraint on the anisotropy in the top 80 km of the inner core beneath the Central Pacific, but the velocity and attenuation anisotropy should exist in the top 180 km of the inner core based on the PKPbc–PKIKP data.

4.5. Possible interpretations

Several possible effects may be attributed to the observed variations of seismic velocity and attenuation in the inner core: temperature, partial melting [9,15], solidification texturing [12,34], and different alignments of the anisotropic hexagonal close-packed (hcp) iron crystals [5,9].

Temperature effect would produce a correlation of high (low) velocity with low (high) attenuation, opposite to our observations. Besides, temperature variations would also be expected to be small because of the large thermal conductivity of the inner core and vigorous convection in the outer core.

Partial melting has been proposed to explain the low Q values and the velocity anisotropy in the inner core [15] and the hemispheric variations in velocity in the top of the inner core [9]. Different geometric inclusions of melt would be required to be able to explain the correlation of high velocity with high attenuation [9]. This mechanism cannot be excluded, but it is difficult to derive a model of melt inclusions and geometry.

Solidification texturing was suggested as a mechanism that may provide one explanation for the velocity anisotropy observed in the polar direction [12,34]. Seismic attenuation may result from the seismic scattering in the solidification textures. This mechanism is similar to the partial melting mechanism and it would be difficult to derive models of solidification textures to explain the variations along different directions and between the two hemispheres.

Variations of travel time and amplitude can also be caused by seismic scattering of a random medium [9,12,22,24,35,36]. Scattering in different types of the medium could also produce a correlation between a smaller travel time and a smaller amplitude. For example, seismic waves propagating in a medium with high background velocity and a large magnitude of velocity variation could result in a smaller travel time and a smaller amplitude than those traveling in a medium with low background velocity and a small magnitude of velocity variation, producing a correlation of high velocity with high apparent "attenuation". Such mechanism, however, cannot explain the direction dependence of seismic velocity and attenuation and their correlation for the seismic waves sampling the same regions of the inner core. Indeed, the PKIKP rays that sample the same region beneath Africa and the Central Pacific but in various directions exhibit strong direction dependence with large PKPbc–PKIKP differential travel times and small PKIKP/PKPbc amplitude ratios observed along polar paths and small PKPbc–PKIKP differential travel times and large PKIKP/PKPbc amplitude ratios observed along equatorial paths. Scattering in a random medium cannot provide an explanation for such observations.

Perhaps, the simplest explanation is that all the observed variations in velocity and attenuation in the inner core are caused by different alignments of the hcp iron crystals. Recent theoretical calculations predict a 10%–12% velocity anisotropy for the single crystal of the hcp iron at inner core temperature [17]. Such magnitude of velocity anisotropy is sufficient to account for the observed differential travel times. To explain the attenuation anisotropy and its relationship to velocity, it would, however, require the hcp iron to be anisotropic in attenuation with the axis of high attenuation

corresponding to that of high velocity. Such hypothesis of attenuation anisotropy in hcp iron crystal remains to be confirmed by either laboratory experiments or theoretical calculations, and the physical mechanisms that may be responsible for these different alignments between the eastern and western hemispheres and between the polar and equatorial directions remain to be explored.

5. Conclusions

We have investigated the attenuation structure of the Earth's inner core and its relationship to the velocity structure globally and along various sampling directions, by studying the amplitude ratios and differential travel times of the PKiKP–PKIKP and PKPbc–PKIKP phases. Our observations reveal that the amplitude ratios of these core phases, like the differential travel times, vary in both sampling direction and geographic location, and the correlation is ubiquitous between small (large) PKIKP/PKiKP or PKIKP/PKPbc amplitude ratios and large (small) differential PKiKP–PKIKP or PKPbc–PKIKP travel times. These observations indicate that the Earth's inner core is anisotropic in attenuation, and the direction of high (low) attenuation corresponds to that of high (low) velocity. In the regions of the western hemisphere of the inner core that exhibit anisotropy, the attenuation anisotropy can be represented by a Q value of about 200–250 along polar paths and an average Q value of 600 along equatorial paths. This attenuation anisotropy corresponds to a polar–equatorial velocity anisotropy with the polar paths being 1.3%–2.8% higher than the equatorial paths. Along equatorial paths, the attenuation structures of the inner core have east–west hemispheric variations with an average Q value of 300 in the eastern hemisphere and an average Q value of 600 in the western hemisphere. Such hemispheric variations in attenuation correspond to hemispheric differences in velocity with the velocity in the eastern hemisphere being about 1% faster than that in the western hemisphere. The above observations can be explained by different alignments of the hexagonal close-packed (hcp) iron crystals under the hypothesis that the hcp iron crystals are anisotropic in attenuation with their axis of high (low) attenuation corresponding to that of high (low) velocity.

Acknowledgements

References

[1] K.C. Creager, Anisotropy of the inner core from differential travel times of the phases PKP and PKIKP, Nature 356 (1992) 309–314.

[2] X. Song, D.V. Helmberger, Depth dependence of anisotropy of Earth's inner core, J. Geophys. Res. 100 (1995) 9805–9816.

[3] S. Tanaka, H. Hamaguchi, Degree one heterogeneity and hemispherical variation of anisotropy in the inner core from PKP (BC)–PKP(DF) times, J. Geophys. Res. 102 (1997) 2925–2938.

[4] X. Song, D.V. Helmberger, Seismic evidence for an inner core transition zone, Science 282 (1998) 924–927.

[5] K.C. Creager, Large-scale variations in inner core anisotropy, J. Geophys. Res. 104 (1999) 23127–23139.

[6] F. Niu, L. Wen, Hemispherical variations in seismic velocity at the top of the Earth's inner core, Nature 410 (2001) 1081–1084.

[7] A. Ouzounis, K.C. Creager, Isotropy overlying anisotropy at the top of the inner core, Geophys. Res. Lett. 28 (2001) 4331–4334.

[8] F. Niu, L. Wen, Seismic anisotropy in the top 400 km of the inner core beneath the "eastern" hemisphere, Geophys. Res. Lett. 29 (12) (2002) doi:10.1029/2001GL014118.

[9] L. Wen, F. Niu, Seismic velocity and attenuation structures in the top of the Earth's inner core, J. Geophys. Res. 107 (B11) (2002) 2273 doi:10.1029/2001JB000170.

[10] L. Stixrude, R.E. Cohen, High-pressure elasticity of iron and anisotropy of Earth's inner core, Science 267 (1995) 1972–1975.

[11] S. Yoshida, I. Sumita, M. Kumazawa, Growth model of the inner core coupled with the outer core dynamics and the resulting elastic anisotropy, J. Geophys. Res. 101 (1996) 28085–28103.

[12] M.I. Bergman, Measurements of elastic anisotropy due to solidification texturing and the implications for the Earth's inner core, Nature 389 (1997) 60–63.

[13] H.-K. Mao, et al., Elasticity and rheology of iron above 220 GPa and the nature of the Earth's inner core, Nature 396 (1998) 741–743.

[14] S.-I. Karato, Seismic anisotropy of the Earth's inner core induced by Maxwell stresses, Nature 402 (1999) 871–873.

[15] S.C. Singh, M.A.J. Taylor, J.P. Montagner, On the presence of liquid in Earth's inner core, Science 287 (2000) 2471–2474.

[16] H.-R. Wenk, S. Matthies, R.J. Hemley, H.-K. Mao, J. Shu, The plastic deformation of iron at pressures of the Earth's inner core, Nature 405 (2000) 1044–1047.

[17] G. Steinle-Neumann, L. Stixrude, R.E. Cohen, O. Gulseren, Elasticity of iron at the temperature of the Earth's inner core, Nature 413 (2001) 57–60.

[18] B.A. Buffett, H.-R. Wenk, Texturing of the Earth's inner core by Maxwell stresses, Nature 413 (2001) 60–63.

[19] V.F. Cormier, Short-period PKP phases and the anelastic mechanism of the inner core, Phys. Earth Planet. Inter. 24 (1981) 291–301.

[20] A. Souriau, P. Roudil, Attenuation in the uppermost inner core from broad-band GEOSCOPE PKP data, Geophys. J. Int. 123 (1995) 572–587.

[21] X. Song, D.V. Helmberger, A P-wave velocity model of Earth's core, J. Geophys. Res. 100 (1995) 9817–9830.

[22] V.F. Cormier, X. Li, G.L. Choy, Seismic attenuation of the inner core: viscoelastic or stratigraphic? Geophys. Res. Lett. 25 (1998) 4019–4022.

[23] X. Li, V.F. Cormier, Frequency-dependent seismic attenuation in the inner core: 1. A viscoelastic interpretation, J. Geophys. Res. 107 (B12) (2002) 2361 doi:10.1029/2002JB001795.

[24] V.F. Cormier, X. Li, Frequency-dependent seismic attenuation in the inner core: 2. A scattering and fabric interpretation, J. Geophys. Res. 107 (B12) (2002) 2362 doi:10.1029/2002JB001796.

[25] S.I. Oreshin, L.P. Vinnik, Heterogeneity and anisotropy of seismic attenuation in the inner core, Geophys. Res. Lett. 31 (2004) L02613 doi:10.1029/2003GL018591.

[26] A. Cao, B. Romanowicz, Hemispherical transition of seismic attenuation at the top of the Earth's inner core, Earth Planet. Sci. Lett. 228 (2004) 243–253.

[27] A. Souriau, B. Romanowicz, Anisotropy in inner core attenuation: a new type of data to constrain the nature of the solid core, Geophys. Res. Lett. 23 (1996) 1–4.

[28] A. Souriau, B. Romanowicz, Anisotropy in the inner core: relation between P-velocity and attenuation, Phys. Earth Planet. Inter. 101 (1997) 33–47.

[29] W. Yu, L. Wen, F. Niu, Seismic velocity structure in the Earth's outer core, J. Geophys. Res. 110 (2005) B02302 doi:10.1029/2003JB002928.

[30] W. Yu, L. Wen, Seismic velocity and attenuation structures in the top 400 km of the Earth's inner core along equatorial paths, J. Geophys. Res. (submitted for publication).

[31] A.M. Dziewonski, D.L. Anderson, Preliminary Reference Earth Model, Phys. Earth Planet. Inter. 25 (1981) 297–356.

[32] D.V. Helmberger, Theory and application of synthetic seismograms, in: H. Kanamori (Ed.), Earthquakes: Observation, Theory and Interpretation, Soc. Italiana di Fisica, Bologna, Italy, 1983, pp. 173–222.

[33] P. Samec, J.P. Blangy, Viscoelastic attenuation, anisotropy, and AVO, Geophysics 57 (1992) 441–450.

[34] M.I. Bergman, Estimates of the Earth's inner core grain size, Geophys. Res. Lett. 25 (1998) 1593–1596.

[35] K. Aki, Scattering of P waves under Montana Lasa, J. Geophys. Res. 78 (1973) 1334–1346.

[36] K. Aki, P.G. Richards, Quantitative Seismology: Theory and Methods, W. H. Freeman, New York, 1980.